Novel MPPT of PV System with MIWO Algorithm for Water Pumping Application

Ramakrishna Raghutu, Vasupalli Manoj and Narendra Kumar Yegireddy

Dr. Ramakrishna Raghutu, Assistant Professor, Department of Electrical and Electronics Engineering, GMR Institute of Technology, Rajam, Vizianagaram, Andhra Pradesh, India – 532127.
Dr. Vasupalli Manoj, Assistant Professor, Department of Electrical and Electronics Engineering, GMR Institute of Technology, Rajam, Vizianagaram, Andhra Pradesh, India – 532127.
Dr. Narendra Kumar Yegireddy, Professor, Department of EEE, Satya Institute of Technology and Management, Vizianagaram, Andhra Pradesh, India – 535003.

Abstract: **The water pumping system (WPS) utilized in this research is powered by a photovoltaic (PV) system and is regulated by an inverter that is equipped with a TS-Fuzzy controller. To enhance the power extraction from the PV system when faced with partial shading conditions (PSCs), a Modified Invasive Weed Optimization (MIWO) technique is incorporated into the Perturb and Observes (P&O) algorithm. The conventional P&O algorithm faces difficulties in harnessing the full potential of the PV system when confronted with partial shading scenarios, primarily because of the presence of numerous maximum points. In such instances, optimization methods can be employed to locate the global maximum point. The MIWO-based P&O algorithm proposed will modify the reference voltage according to the prevailing weather conditions in order to guarantee optimal operation of the PV system at the Maximum Power Point (MPP). The PV-based WPS is designed to cater to both irrigation and domestic water supply needs. In this study, a sensorless vector control-based induction motor is utilized to drive the pump. The primary goal of this study is to showcase the efficiency of a PV-based WPS without the necessity of battery storage. The TS-Fuzzy controller guarantees smooth motor operation during transient periods. The efficacy of the proposed approach is confirmed through MATLAB/Simulink simulations as well as Hardware – in the – Loop and real-time data is also used, taking into account various water pumping scenarios and the fluctuating solar irradiance levels during rapid climate changes.**

Keywords **–MPPT, Modified Invasive Weed Optimization (MIWO), Photovoltaic (PV) System, Water Pumping System.**

Corresponding Author: ramakrishna.r@gmrit.edu.in

Acknowledgement:
The authors would like to thank the management of GMR Institute of Technology, Rajam, Vizianagaram for the constant support and encouragement rendered by them and also for providing us various facilities including OPAL-RT devices to achieve the outcome of this research paper.

1. INTRODUCTION

WPSs are essential for the discharge of water in our daily lives. However, they consume a substantial amount of electrical energy. With the increasing focus on environmental issues and the necessity to decrease CO_2 emissions, there is a growing interest in renewable energy sources. Photovoltaic (PV) cells are among the most promising devices as they provide an eco-friendly solution to generate electricity from sunlight. One practical application of PV systems is in WPS for irrigation and domestic purposes. These systems are particularly favoured in regions where grid access is limited or costly [1-3].

Various approaches to PV-based WPSs have been suggested in previous studies. While some have utilized Brushless DC (BLDC) motors, these are not suitable for agricultural purposes due to their high cost and maintenance requirements. Other studies have focused on the use of Permanent-Magnet Synchronous Motors (PMSM) powered by single-stage PV systems, with an emphasis on optimizing the operation of the inverter. Furthermore, the performance of reluctance motors under partially shaded conditions has been examined for WPSs. Induction motors have also been considered for pumping, and efforts have been made to develop systems with battery storage for residential applications. However, it is important to note that implementing such systems in single-phase residential areas can incur higher costs and necessitate additional maintenance due to the presence of batteries.

An efficient solution is vital to ensure that the PV generator operates at its highest power point (MPP), resulting in a highly effective system [4-14]. This can be accomplished by utilizing a Maximum Power Point Tracker (MPPT) converter with an efficient methodology. MPPT plays a vital role in PV systems as it effectively lowers the overall cost of the array by minimizing the required number of solar panels to attain the desired power output. The power output of PV systems typically fluctuates due to weather conditions, which is why battery integration is necessary for flexible operation. However, integrating batteries increases the overall system cost and requires regular replacement and maintenance [2]. An alternative approach is to operate the system without energy storage, meaning without a battery. In this research, we examine a PV-based WPS without a battery and propose an effective control strategy to operate the system under various conditions. MPPT can be accomplished by controlling either the PV voltage or the dc-link voltage, particularly at the voltage corresponding to the maximum power point (MPP) as determined by the perturb and observe (P&O) methodology. However, the conventional P&O algorithm is unable to accurately track the MPP under PSC of the PV system due to the presence of multiple local maximum points of power. Hence, it is imperative to ascertain the global maximum point in order to derive the utmost power output from the PV system. This can be accomplished by integrating evolutionary optimization techniques [15-16] into the conventional P&O algorithm. The Invasive Weed Optimization (IWO) algorithm is a method that takes cues from the behavior of colonizing weeds, showcasing improved robustness, adaptability, and randomness akin to those of colonizing weeds [17]. The IWO algorithm conducts a search based on exceptional individuals within the population group and offers the following advantages [17-18].

1. The IWO algorithm possesses the capability to generate fresh weeds from all existing weeds. Weeds that exhibit the highest fitness value have the potential to produce a larger quantity of weeds in close proximity to their parent weed. Consequently, this attribute significantly improves the convergence of the IWO algorithm.

2. The search space is characterized by a normal distribution, which determines the distribution of the new weeds. By generating random numbers through this distribution, it is ensured that no two weeds can occupy the same position without mating. This distinctive attribute of IWO enables a comprehensive exploration of the entire search space.

The aforementioned characteristics enable IWO to efficiently search for the global maximum even in situations of PSC in PV systems. The integration of P&O with IWO algorithms offers a viable solution. This paper presents the implementation of an integrated algorithm, combining MIWO with P&O, to extract the maximum power from PV systems under PSCs. The MIWO-based P&O algorithm proposed modifies the reference voltage in order to enhance the operation of the PV system at the peak power point, considering the prevailing weather conditions. Typically, submersible pumps are utilized in WPSs, resulting in the motor being located at significant depths. Consequently, accurately sensing the motor's speed becomes challenging and not advisable. In order to tackle this problem, the paper examines the use of a sensorless vector control-based induction motor for operating the pump.

2. WATER PUMPING SYSTEM

The WPS operated by PV is commonly used in distributed energy generation systems [2, 11-13]. Numerous experimental dc motor driven PV pumps are currently being utilized globally; however, they encounter maintenance challenges because of the commutator and brushes. As a result, an Induction Motor (IM) based pumping system presents itself as an attractive option, providing reliability and maintenance-free operations. To drive the IM from the PV system, an inverter is necessary. Furthermore, it is necessary to have a DC to DC circuit in order to optimize power extraction from the photovoltaic system. To mitigate the impact of weather conditions [2, 20] on the WPS, an energy storage device such as a battery is necessary. However, the inclusion of an extra dc/dc circuit and battery can increase the overall system cost [2, 21]. These challenges can be addressed by implementing a proper controller for the inverter, eliminating the need for a dc/dc converter and battery. The proposed controller can function as an MPPT converter for the PV system, ensuring maximum power extraction without the requirement of an additional dc/dc converter. Furthermore, the proposed inverter control can maintain power balance between PV generation and load (i.e., power consumed by the IM), eliminating the need for a battery to maintain power equilibrium between generation and load.

Submersible pumps are commonly utilized in PV-based WPS for medium head applications [22]. These pumps are fully submerged underwater, including the motor. Consequently, detecting the speed using a speed sensor becomes challenging and costly due to the motor-pump being underwater. Hence, this study focuses on implementing sensorless speed control of an induction motor (IM) for PV-based WPS.

Several researchers have previously presented a PV-based WPS that is similar to the one described. In their work [2], the authors proposed a WPS that does not include energy storage or a dc/dc converter. However, they did not take into account the PSC on the PV system. Conversely, the WPS outlined in [11] utilizes solar panels and a battery for operation. Interestingly, in [2, 11-13], the authors did not consider the PSC and also did not apply optimization techniques. Additionally, the authors utilized a speed sensor to measure the speed of the IM. The system under consideration is depicted in Figure 1.

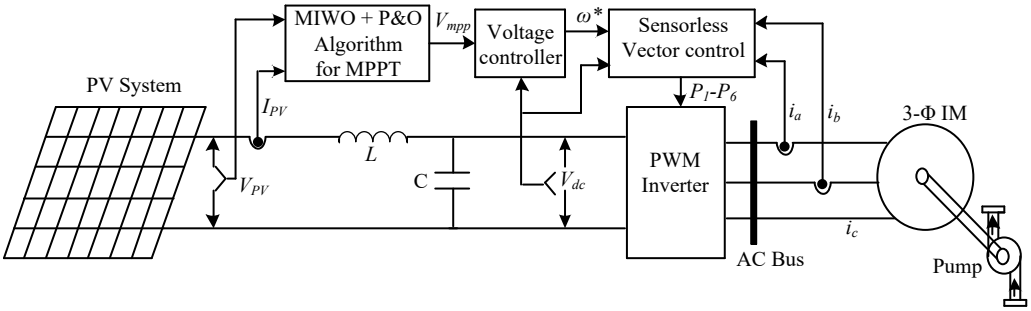

Fig. 1: PV base WPS without energy storage.

3. SYSTEM DISCRIPTION

a) PV System

Figure 2(a) illustrates the diagram of a PV cell. The PV array consists of numerous PV cells that are interconnected in both series and parallel arrangements. Figure 2(b) depicts the PV array under PSCs. The current-voltage characteristic function [11-13] describes the behavior of the PV array.

$$I_{PV} = n_p I_{ph} - I_{rs}\left[\exp\left(\frac{q(V_{PV} + I_{PV}R_s)}{AKTn_s}\right) - 1\right] - \frac{V_{PV} + I_{PV}R_s}{R_{sh}} \quad (1)$$

In accordance with the P-V characteristics of a PV system, the maximum power can be generated at a specific voltage known as the voltage at maximum power point (V_{MPP}). Figure 3 (a) depicts the P-V characteristics at various levels of irradiance, assuming a uniform irradiance. On the other hand, Figure 3 (b) illustrates the P-V characteristics under different PSC, with the corresponding PSC values listed in Table-1. Among the various algorithms proposed in the literature, the P&O algorithm is the most widely used technique for maximum power point tracking (MPPT) [1-2, 11-15, 23-24].

The direction for additional perturbation is determined by the P & O algorithm according to the sign of the power change. To ensure that the output voltage aligns with its reference, a feedback control loop is implemented. The voltage at which the maximum power point (MPP) is achieved is determined using the following equation.

$$V_{mpp}(i) = \Delta V \times \text{sign}\left(\frac{dP_{PV}}{dV_{PV}}\right) + V_{mpp}(i-1) \quad (2)$$

where, 'i' is the iteration and ΔV is steep voltage.

Nevertheless, the conventional P&O algorithm proves inadequate in accurately tracking the optimal point under PSCs due to the presence of numerous local maximum power points, as depicted in Figure 3(b). Hence, the utilization of the MIWO technique enables the efficient detection and monitoring of the highest global point of power among all the existing maximum power points.

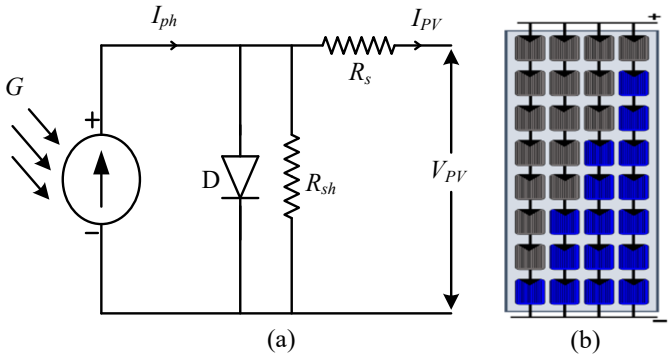

Fig. 2: PV (a) cell (b) array under partial shading.

Table 1: Patrons of irradiances (**Fig. 2(b)**).

Pattern	PV string.
1	[*Uniform*]: **Fig. 3(a)**; Module: 1-22= 200.0 to1000W/m^2.
2	[*PSC*-1]: **Fig. 3(b)**; Module: 1–2=1000W/m^2; 3–8=810W/m^2; 9–18=605W/m^2;19–22=406W/m^2.
3	[*PSC*-2]: **Fig. 3(b)**; Module: 1=998W/m^2; 2–5=800W/m^2; 6–12=590W/m^2; 13–22=400W/m^2.

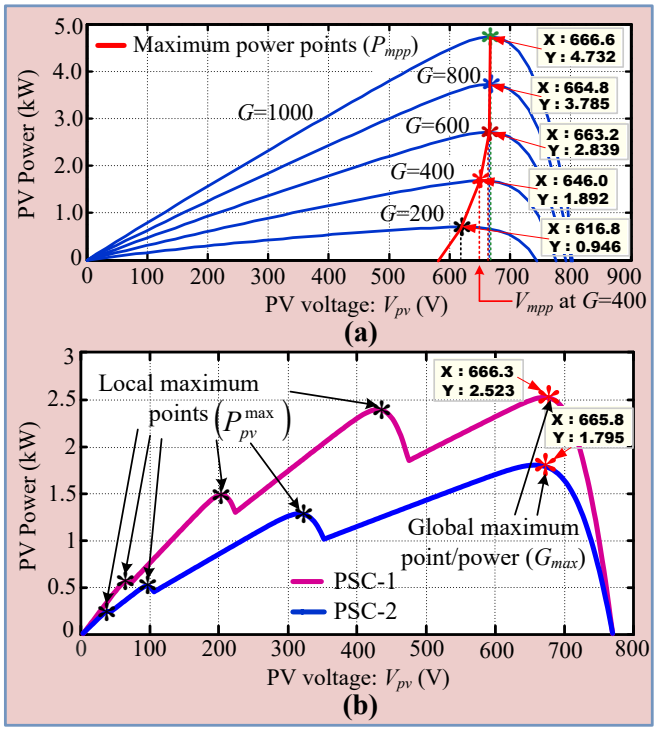

Fig. 3: *P-V* characteristics **(a).** Uniform solar irradiance, **(b).** Under partial shading.

b) Motor-Pump set

The effectiveness of the submersible pump is determined by its head-flow rate curve while in operation at the specified speed. The speed of the impeller directly affects the flow rate, whereas the head is proportional to the square of the speed. Furthermore, the hydraulic power increases in direct proportion to the cube of the velocity. These curves precisely showcase the pump's performance at high speeds, but their accuracy may vary at lower speeds or when utilized with a constant head. At very low speeds, the pump's pressure output is lower than the static pressure, causing the water to circulate within the pump without being delivered. Therefore, a minimum speed or threshold speed is necessary to ensure water delivery. It is important to note that excessively high motor speeds can lead to damage in both the motor and pipes due to increased pressure. To prevent this, a proposed controller has been designed to operate the motor within permissible limits. The controller will automatically stop the motor if its speed falls below the lower limit by disabling the pulses to the inverter. Upon reaching a certain speed limit or initial value, the pump will commence the water delivery process, and the flow rate (Q, liter/min) will change proportionally with the speed (ω) [13], as indicated in equation (3).

$$Q = a\omega - b, \omega \geq \omega_t \text{ and } Q = 0, \omega < \omega_t \quad (3)$$

4. IWO ALGORITHM

The innovative weed optimization method, developed by Mehrabian and Lucas in 2006 [25], presents a distinct strategy for optimization that is inspired by the colonization behavior of weeds. Over the past ten years, it has garnered significant interest from researchers. Its remarkable attributes, such as reproduction, spatial dispersal, and competitive exclusion, set it apart from other cutting-edge evolutionary algorithms. As a result, it has found applications in various fields of Engineering and Sciences. The IWO process encompasses the following steps:

Step-1: *Version 1: The search space is randomly populated with a finite number of individuals during the initialization phase.*

Step-2: *Reproduction:* Every weed in the population is granted the opportunity to generate new weeds after entering a flourishing tree. The quantity of fresh weeds produced by a potential weed is determined by its relative highest and lowest levels of fitness. It is linearly decreases from an allowable maximum weeds ($S_{\max}$) to minimum weeds (S_{mim}) with $S_{\max}$ for the best candidate weed, S_{mim} for the worst participated weed in the population.

$$n(w_i) = \frac{S_{\max}(\max\ fit - fit(w_i)) + S_{\min}(fit(w_i) - \min\ fit)}{\max\ fit - \min\ fit} \quad (4)$$

Step-3: *The distribution of the newly generated weeds across the search space follows a normal distribution. The mean of the parent weed position is used as the center of this distribution, while the standard deviation varies and is defined as.*

$$\sigma_{gen} = (\sigma_{\max} - \sigma_{\min}) \frac{(gen_{\max} - gen)^{mi}}{gen_{\max}^{mi}} + \sigma_{\min} \quad (5)$$

The standard deviation (SD) at the current generation is denoted as (σ_{gen}), while ($\sigma_{\max}$) and ($\sigma_{\min}$) represent the maximum and minimum standard deviations, respectively. These values are predefined parameters. $gen_{\max}$ signifies the maximum number of generations. The nonlinear modulation index is represented by (NM) and the need for generated seeds to be close to the parent weed is emphasized.

Step-4: Competitive Exclusion: In the absence of offspring, a plant would face extinction, whereas if it does produce offspring, it has the potential to dominate the world. This phenomenon is observed in certain weed species in the field, where competition occurs to regulate the weed population. When the combined number of parent weeds and newly generated weeds surpasses the maximum limit (W_{max}), the weeds with the lowest fitness value are systematically eliminated from the population until it reaches W_{max} .

Step-5: *Termination Condition:*

1) The current iteration is equivalent to the maximum number of iterations.
2) The maximum number of fitness evaluations has been reached by the above process (Steps 1-4).
3) $\left|f(x^*)-f(x)\right|\le\varepsilon$ If any of the conditions mentioned above (Steps 1-4) are met, the process will be halted. The user defines the small tolerance value, while the best solution obtained by the present method is compared to the best known optimal solution.

The IWO algorithm commonly utilizes the Gauss function. During the reproduction phase of the IWO algorithm, offspring are produced by overlaying the Gaussian distribution of random variables onto the parent individual. To achieve optimal reproductive performance, it has been observed that the Cauchy distribution function yields better results compared to the Gauss distribution [17, 26]. Figure 5 illustrates the probability density functions of the Cauchy and Gauss distributions, as per their definitions [17, 26].

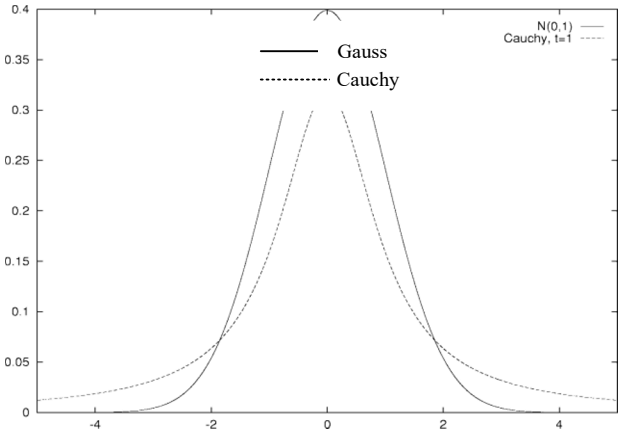

Fig. 5: Cauchy and Gauss function [17, 26].

According to Figure 5, it is evident that the Cauchy distribution is smaller in size compared to the Gaussian distribution when looking at the vertical axis. Moreover, when the Cauchy distribution is in close proximity to the horizontal axis, it becomes wider in the horizontal direction. Consequently, the Gaussian distribution function has a greater likelihood of generating minor perturbations rather than significant disturbances [17]. Conversely, the Cauchy distribution function possesses a lesser capacity for perturbations compared to the Gaussian function, but it is more effective in generating substantial disturbances. Moreover, it is evident from Figure 5 that the Cauchy mutation has a tendency to produce offspring that are farther from their parent in comparison to the Gaussian mutation, mainly because of its elongated tails. It can be inferred from this observation that the Cauchy distribution has a higher tendency to escape a local optimum or move away from a plateau, especially when the "basin of attraction" of the local optimum or plateau is significantly larger than the average steepness [26]. Consequently, the Cauchy

distribution is more effective in preserving population diversity and enhancing the global optimization and dependability of the algorithm. As a result, the IWO algorithm utilizes the Cauchy distribution function rather than the Gaussian distribution function, leading to the creation of the Modified IWO (MIWO) algorithm. Since weather conditions tend to change rapidly, the MIWO algorithm is implemented in this paper.

The Cauchy density function, which is centered at the origin, is defined by [26].

$$f(x)=\frac{1}{\pi}\frac{t}{t^2+x^2}, \qquad -\infty<x<\infty \tag{6}$$

The distribution function [26] corresponds to a scale parameter t > 0.

$$F(x)=\frac{1}{2}+\frac{1}{\pi}\arctan\left(\frac{x}{t}\right) \tag{7}$$

The MIWO algorithm generates W_{max} seeds around the parent seed, following the same principle, W_{max} voltage points are generated around the previous voltage value. Additionally, the P&O algorithm is utilized to generate a new voltage value. As a result, W_{max} new calculated PV currents can be obtained from W_{max} voltage values. Consequently, W_{max} power points can be calculated, leading to the optimization of P_{PV}^{max}. This process continues until the search space is fully explored. The new value of voltage can be obtained through this iterative process.

$$V_{new}^{i}=V_{old}^{i}+m\sigma_{gen}\delta_i, \quad i=1,....,\ W_{max} \tag{8}$$

where, δ_i is a Cauchy random variable and $m=\Delta V\times \text{sign}\left(\frac{dP_{PV}^{max}}{dV_{mpp}}\right)$

Figure 6 displays the flowchart of the proposed system.

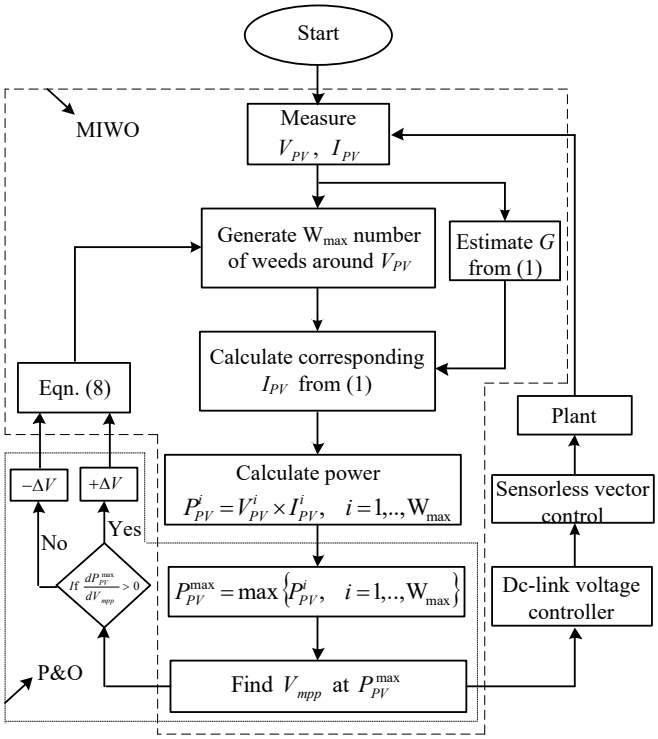

Fig. 6: Flowchart of proposed system.

5. Control of Voltage and Induction Motor Speed

A) Control of voltage at dc-link:

The power imbalance between generation and load can result in changes in certain factors. The power generated by a photovoltaic (PV) system is dependent on the V_{mpp} (maximum power point voltage). In the case of an induction motor (IM) with a constant head (water depth), the torque remains constant. As a result, the power consumed by the IM (load power) is solely dependent on the motor's speed. The reference dc-link voltage, achieved through the MIWO plus P&O algorithm (V_{mpp}), is compared to V_{dc}. The resulting error is then fed into a PI controller. The reference speed (required speed) of the IM is determined by the output of the PI controller. This signal serves as the input for the sensorless vector control block, as depicted in Figure 7. A limiter is employed to restrict the reference speed generated by the PI controller, as shown in Figure 7. This ensures that the speed of the IM remains within acceptable limits. If V_{dc} exceeds V_{mpp}, it indicates that there is excess power available on the generation side. Consequently, the controller (PI) must increase the reference speed signal. To achieve this, negative gains are necessary for the PI controller, or alternatively, the error should be multiplied by a gain of '-1'. In this study, the ITSE [27] method is utilized to tune the gains of the PI controller.

B) TS-Fuzzy Controller

The TS-fuzzy controller, due to its variable linguistic rule consequent and infinite gain variation characteristics, is capable of effectively addressing complex control problems. The stability of the power system is improved and the monitoring of system uncertainties is effectively carried out during changes in weather conditions and variations in load [34-35]. Furthermore, it has been noted that the TS-fuzzy controller offers a superior control solution for nonlinear control issues and system uncertainties across different operating conditions when compared to the PI-controller [34-35]. Therefore, in order to enhance the dynamic performance of the system, the study utilizes the TS-fuzzy based controller. Figure 7 illustrates a model of the TS-Fuzzy system.

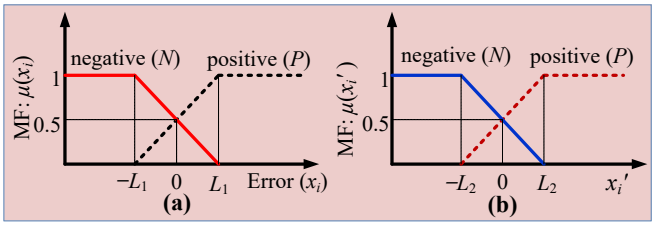

Fig. 7: MFs for**: (a).** error signal (x_i) and **(b).** Derivative of error signal (x_i').

The discrepancies in current/voltage error (x_i) & its derivative (x_i') signal serve as the input variables for the fuzzy control system in order to design the TS-fuzzy controller(s), as illustrated in Figures 5 and 8. The input voltage/current error and its derivative signals are transformed into fuzzy values using two linguistic memberships (MFs) values; P for positive and N for negative, as shown in Figure 7. The MFs for the two input linguistic variables; P and N for x_i and x_i' signals are represented by equations (5) and (6) respectively.

$$\mu_P(x_i)=\begin{cases}0, & x_i<-L_1\\ \dfrac{x_i+L_1}{2L_1}, & -L_1\le x_i\le L_1\\ 1, & x_i>L_1\end{cases} \text{ and } \mu_N(x_i)=\begin{cases}1, & x_i<-L_1\\ \dfrac{-x_i+L_1}{2L_1}, & -L\le x_i\le L_1\\ 0, & x_i>L_1\end{cases} \quad (5)$$

$$\mu_P(x_i')=\begin{cases}0, & x_i'<-L_2\\ \dfrac{x_i'+L_2}{2L_2}, & -L_2\le x_i'\le L_2\\ 1, & x_i'>L_2\end{cases} \text{ and } \mu_N(x_i')=\begin{cases}1, & x_i'<-L_2\\ \dfrac{-x_i'+L_2}{2L_2}, & -L\le x_i'\le L_2\\ 0, & x_i'>L_2\end{cases} \quad (6)$$

The simplified four fuzzy rules represent the TS-fuzzy controller:

***Rule*-1:** If $x_i(\kappa)$ is N and $x_i'(\kappa)$ is N, # $Z_1=a_1x_i'(\kappa)+a_2x_i'(\kappa)$.

***Rule*-2:** If $x_i(\kappa)$ is N and $x_i'(\kappa)$ is P, # $Z_2=b_1Z_1$.

***Rule*-3:** If $x_i(\kappa)$ is P and $x_i'(\kappa)$ is N, # $Z_3=b_2Z_1$.

***Rule*-4:** If $x_i(\kappa)$ is P and $x_i'(\kappa)$ is P, # $Z_4=b_3Z_1$.

The subsequent of the TS-fuzzy controller is represented by $Z_{1\text{-}4}$ in the aforementioned rules. The kth sampling instant is denoted by k. The fuzzy constants, namely $a_{1\text{-}2}$, $b_{1\text{-}3}$, are listed in the Appendix. Additionally, the proportional (K_p) and integral (K_i) parameters of the PI-controller are provided in the Appendix. The design of the PI-controllers' coefficients is based on the integral-square-error (ISE) performance criteria, as stated in [35].

The TS-fuzzy controller produces the output (Y) by utilizing the generalized defuzzifier, which is assessed in the following manner:

$$Y=\frac{(Y_1\times Z_1+Y_2\times Z_2+Y_3\times Z_3+Y_4\times Z_4)}{(Z_1+Z_2+Z_3+Z_4)} \quad (7)$$

The dynamic adaptation of the value of 'Y' through the implementation of a fuzzy-based controller enhances the stability of the power system during system events or contingencies.

C) Sensoreless speed control of Induction motor:

In general, the control of an induction motor (IM) can be working based on various methods such as $\frac{v}{f}$ control, indirect field oriented control (IFOC), or vector control and slip control [2, 28-36]. The slip and IFOC control techniques ensure the decoupling between the controllers of torque and flux. Among these controllers, IFOC is a simple and suitable option for WPSs [2, 12-13]. As previously mentioned, sensorless control has advantages in submersible WPSs, and in this paper, sensorless vector control is implemented. The block diagram in Figure 8 illustrates the sensorless speed control of the IM. In sensorless speed control, accurate speed estimation is crucial and can be achieved through mathematical expressions [28, 34-36]. Estimating speed requires the input voltage and currents of the IM. As a result, both voltage and current sensors are essential. In addition, a pair of present sensors is sufficient for detecting the currents of the three phases. Furthermore, the input voltages can be obtained through the phase voltage reconstruction block depicted in Figure 8. The output of the inverter, which serves as the input of the IM, depends on both V_{dc} the modulation index and the pulses generated by the PWM generator. Consequently, the inverter voltages can be obtained using mathematical expressions [36]. Consequently, there is no need for physical voltage sensors to detect the input voltage of the IM, leading to a more economical system.

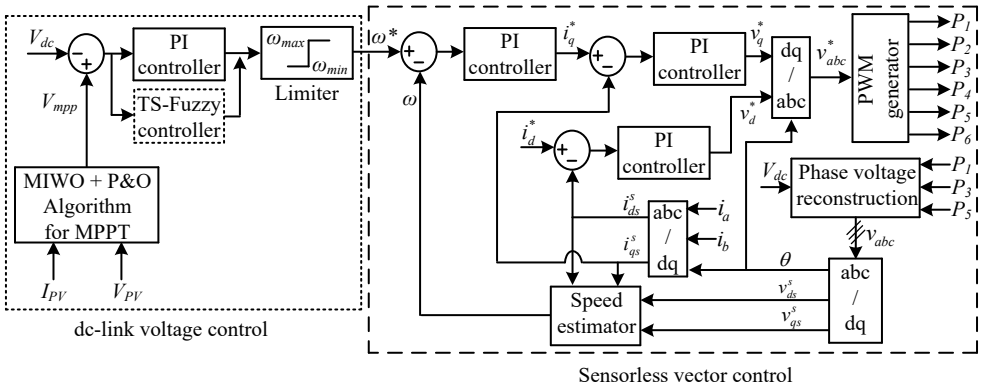

Fig. 8: Proposed control for PV based WPS.

Speed can be estimated by following equations [28, 34-36]:

$$v_{ds}^s = i_{ds}^s R_s + L_{ls}\frac{d}{dt}\left(i_{ds}^s\right) + \frac{d}{dt}\left(\psi_{dm}^s\right) \tag{9}$$

$$v_{ds}^s = \frac{L_m}{L_r}\frac{d}{dt}\left(\psi_{dr}^s\right) + \left(R_s + \sigma L_s S\right) i_{ds}^s \tag{10}$$

where, $\sigma = 1 - \dfrac{L_m^2}{L_r L_s}$

$$\frac{d}{dt}\left(\psi_{dr}^s\right) = \frac{L_r}{L_m} v_{ds}^s - \frac{L_r}{L_m}\left(R_s + \sigma L_s S\right) i_{ds}^s \tag{11}$$

Similarly

$$\frac{d}{dt}\left(\psi_{qr}^s\right) = \frac{L_r}{L_m} v_{qs}^s - \frac{L_r}{L_m}\left(R_s + \sigma L_s S\right) i_{qs}^s \tag{12}$$

$$\frac{d}{dt}\left(\psi_{dr}^s\right) = \frac{L_m}{T_r} i_{ds}^s - \omega_r \psi_{qr}^s - \frac{1}{T_r}\psi_{dr}^s \tag{13}$$

$$\frac{d}{dt}\left(\psi_{qr}^s\right) = \frac{L_m}{T_r} i_{qs}^s + \omega_r \psi_{dr}^s - \frac{1}{T_r}\psi_{qr}^s \tag{14}$$

where, $T_r = \dfrac{L_r}{R_r}$

Moreover, angle of rotor will be obtained by following equation.

$$\theta_e = \tan^{-1}\left(\frac{\psi_{qr}^s}{\psi_{dr}^s}\right) \tag{15}$$

Hence, rotor speed is calculated by below equation,

$$\omega_r = \frac{d}{dt}\theta_e = \frac{1}{\psi_r^2}\left[\left(\psi_{dr}^s \frac{d}{dt}\psi_{qr}^s - \psi_{qr}^s \frac{d}{dt}\psi_{dr}^s\right) - \frac{L_m}{T_r}\left(\psi_{dr}^s i_{qs}^s - \psi_{qr}^s i_{ds}^s\right)\right] \tag{16}$$

Slip speed can be estimated by below equation,

$$\omega_{slip} = \frac{\left(1+\sigma T_r S\right) L_s i_{qs}}{T_r\left(\psi_{ds} - \sigma L_s i_{ds}\right)} \tag{17}$$

Hence,

$$\omega = \omega_{slip} + \omega_r \tag{18}$$

The complete block diagram of speed estimation with the help of equation from (9) to (18) is shown in Fig. 9.

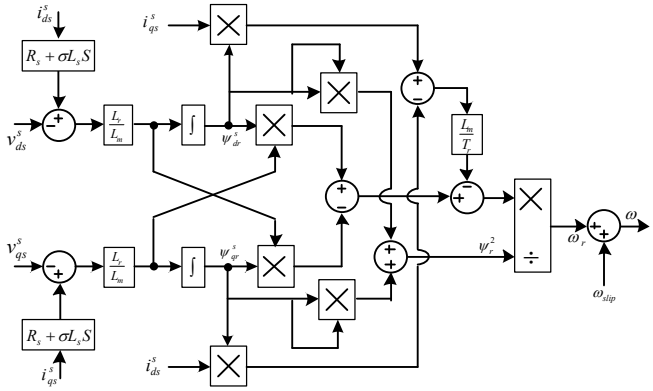

Fig. 9: Speed estimation block.

Estimated speed (ω) will be compared to reference speed (ω^*) which is generated by dc-link voltage control. The error will be given to PI controller. PI controller generates reference quadrature axis current (i_q^*). Reference current of direct axis (i_d^*) can be obtained from reference flux. Reference voltages of quadrature and direct axis (v_q^* and v_d^*) are estimated through PI controllers by comparing corresponding axis currents to its references as shown in Fig. 7. Pulses for inverter are generated from PWM generator with the help of reference voltages (v_{abc}^*) as shown in Fig. 7.

6. Simulation and HIL Results and Discussions

Simulation results were conducted using MATLAB/Simulink. Typically, WPSs utilize 3-phase induction motors with a capacity rating ranging from 0.5 hp to 30.0hp, depending on the head and maximum water discharge [37]. However, in many parts of India, 5 hp motors are employed for WPS in irrigation systems [38]. For this particular study, a 5.0hp induction motor was chosen with a head of 25 m and a maximum water discharge of 300 lit/min. The PV array for the 5 hp motor was rated at 4.7kW, consisting of 22 solar modules connected in series. Detailed parameters for the PV module, induction motor, and MIWO can be found in the Appendix. Once obtained the simulation model, the model is dumped into OPAL-RT model by using below process to establish a Hardware – in the – Loop (HIL).

Real-time simulators (RTSs) modules have the ability to efficiently run complex systems in real-time by rapidly solving power system equations. This allows it to continuously generate output conditions that accurately represent the conditions in the actual network [1]. The RTS technology has gained widespread acceptance as an excellent tool for designing, developing, and testing of various power system control schemes. In order to implement the HIL setup, researchers have utilized two RTS modules developed by OPAL-RT technologies. Unit-1 houses the full plant model, whereas unit-2 houses the recommended control method. Both units are equipped with analog and digital cards to

make a loop by interconnecting them. The control unit will receive the analog signals from the plant, while digital signals are sent from the control to the plant. Extensive results are extracted through another computer for the examination of results under various operating conditions. The configuration of the HIL setup using two OPAL RT-OP5700 modules can be seen in Figure 10. Furthermore, the outcomes are presented in the subsequent case studies.

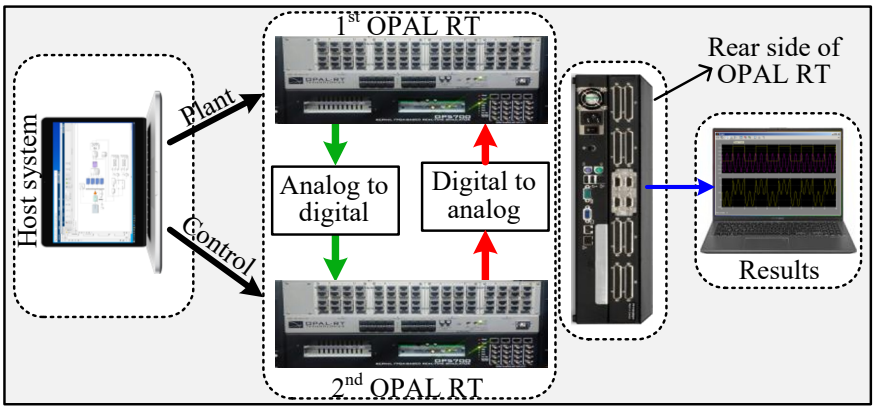

Fig. 10: HIL architecture.

Case-1: *MPPT under change in irradiance*

The irradiance level changes from 1000W/m2 to 900W/m2 at t V_{mpp} =2 sec. The MPPT algorithm successfully tracks the proper V_{mpp} to achieve maximum power. The proposed controller operates at V_{mpp}, ensuring that the system operates at its maximum possible power. The corresponding responses are illustrated in Figure 11. Figure 11(a) displays the change in irradiance and the corresponding V_{mpp} generated by the proposed MPPT algorithm, as shown in Figure 11(b). Nevertheless, the reduction in irradiance may lead to a temporary drop in the dc-link voltage, as illustrated in Figure 11(c). Consequently, the MPPT algorithm momentarily increases the reference voltage, as shown in Figure 11(b) after t=2 sec. Once the dc-link voltage starts to increase, the MPPT algorithm attempts to reduce the reference voltage through voltage steps, following Equation (2). The input to the dc-link controller is provided by this reference voltage, while the inverter controller, as shown in Figure 11(c), regulates V_{dc} at V_{mpp}. Figure 10(d) illustrates the associated power. By observing Figure 11(d), it is evident that the power produced by the PV system aligns with its reference power. Consequently, the inverter acts as an MPPT converter, removing the necessity for an extra dc/dc converter to optimize power extraction from the PV system. With the decrease in power output from the PV system, the suggested controller diminishes the reference speed signal produced by the dc-link voltage controller, leading to a reduction in the speed of the IM.

Case-2: *MPPT under partial shading*

In most cases, PV arrays do not receive uniform irradiance. Consequently, partial shading leads to the formation of numerous local maximum power points. The MIWO based MPPT algorithm proposed guarantees the attainment of the correct 'V_{mpp}' value, aligning with the worldwide maximum power. This feature enables the system to function at the peak power point even when faced with partial shading circumstances. Conversely, the traditional P&O algorithm can solely capture the voltage linked to the initial local

minimum, situated near the current voltage point. Therefore, the combination of the P&O algorithm and the MIWO algorithm has the potential to significantly improve efficiency and extract additional power from the PV system in various scenarios.

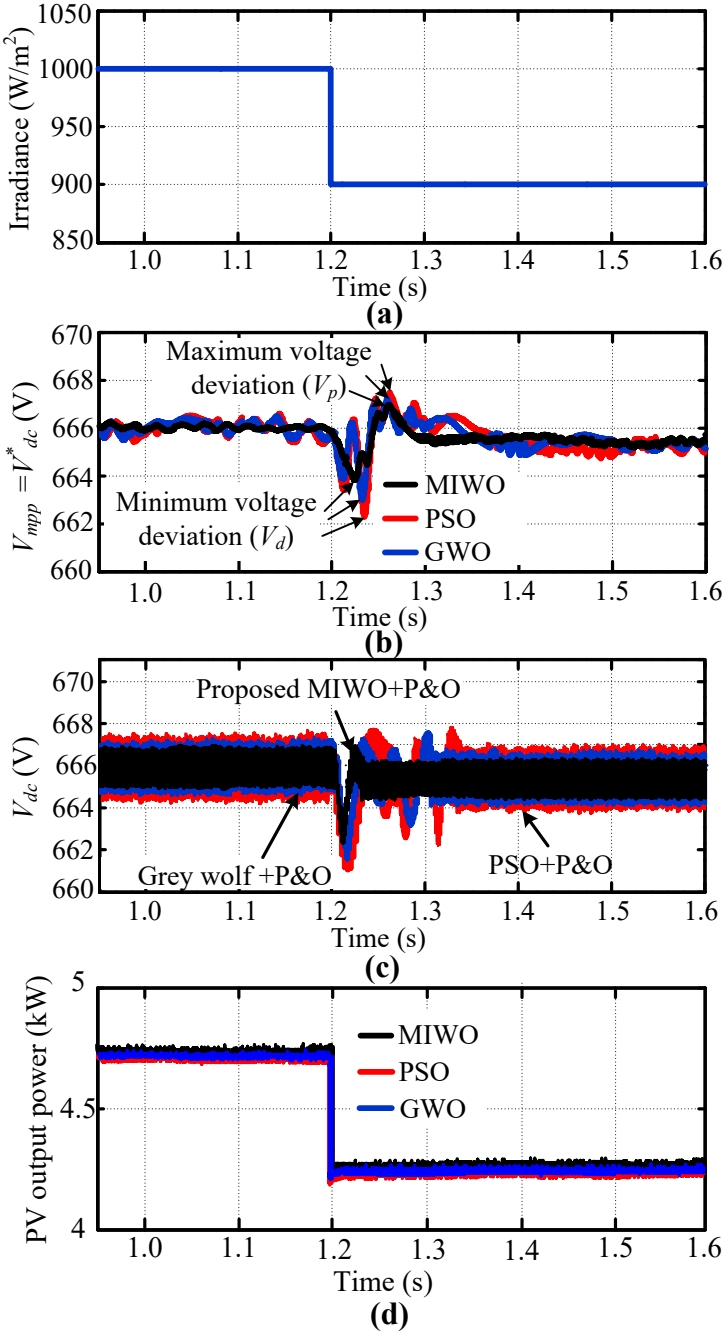

Fig. 11: (a) Change in irradiance, (b) V_{mpp}, (c) V_{dc} (d) Powers.

At the 6-second mark, the presence of partial shading is now being recognized. The PV power corresponding to this is depicted in Figure 12. Upon examination of the information presented in Figure 12, it is evident that the power produced by the PV system aligns with

the maximum potential power, even when partial shading is present. Hence, the proposed controller possesses the ability to extract the highest possible power from the PV system.

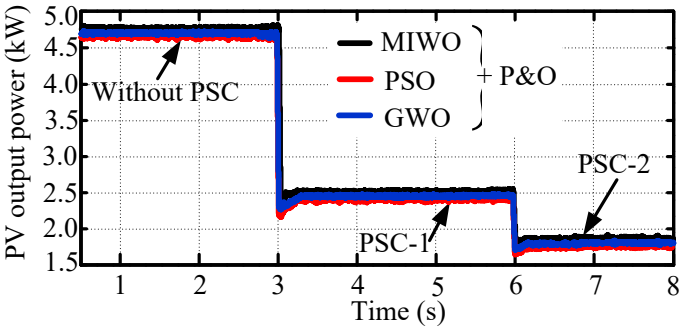

Fig. 12: PV power under partial shading.

Case-3: U*nder normal operation*

In this case, results are obtained when uniform irradiance distributed over PV system under experimental validations. Real time parameters which listed in Appendix are considered in this section. Hence, there is no change in current and Voltage generated by PV system. Therefore, PV system produces constant power. Corresponding I_{PV}, V_{PV} and P_{PV} are shown in Fig. 13. For this available irradiance, V_{mpp} is tracked as 136.5V by controller, hence, controller operates dc-link voltage at 136.5V as shown in Fig. 13(b). Correspondingly PV generates 680W as shown in Fig. 13(c).

Case-4: U*nder partial shading condition*

In this scenario, a uniform irradiance is initially taken into account, and then partial shading is introduced. The resulting power is depicted in Figure 14. The power output of the photovoltaic (PV) system decreases when partial shading occurs. However, the controller continuously monitors and adjusts to maximize the available power from the PV system. Prior to the partial shading, the PV system generates approximately 960W, but after the shading is introduced, it stabilizes at around 740W.

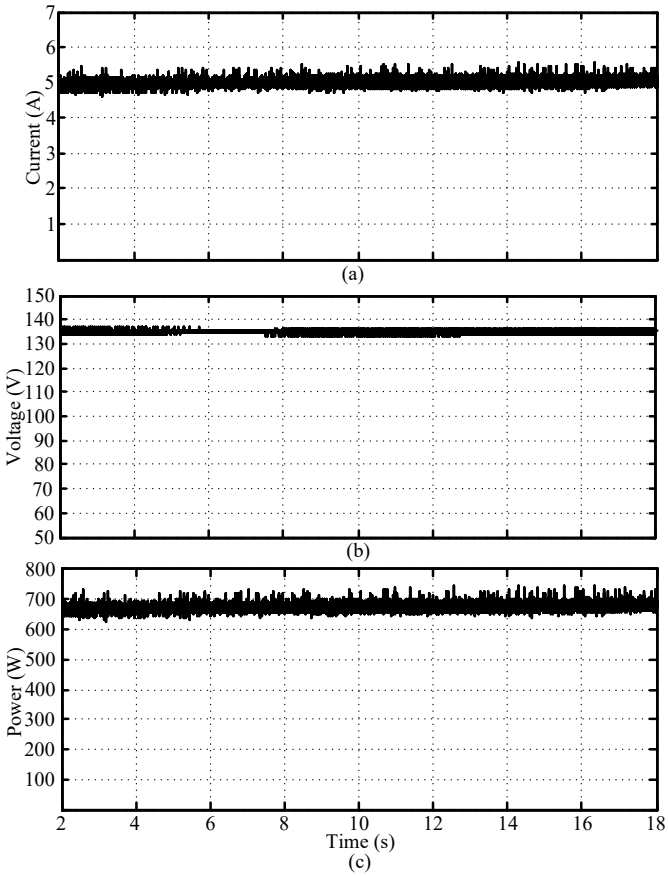

Fig. 13: PV (a) current, (b) dc-link voltage, (c) power.

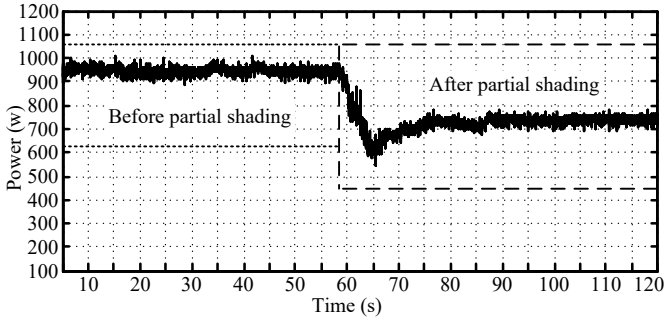

Fig. 14: PV power.

7. CONCLUSSIONS

This document introduces a WPS based on photovoltaic technology that utilizes an IM without the need for energy storage. It incorporates sensorless vector control and an integrated MPPT algorithm. The proposed system provides a cost-effective alternative to systems that require energy storage, speed sensors, and AC voltage sensors. By employing an innovative inverter control technique, the power balance between the PV array and the load is maintained by regulating the speed of the IM to keep the dc-link voltage constant at its reference value (V*dc) within acceptable limits. The integrated MPPT algorithm, in

conjunction with the MPPT-inverter controller, ensures that the PV system operates at peak power levels even under conditions of partial shading, eliminating the necessity for an additional dc/dc converter. The controller's performance has been validated using real-time data, as detailed in this paper. The suggested unified controller solely requires measurements of the dc-link voltage, dc current, and load currents, thereby eliminating the requirement to monitor the IM speed and AC bus voltages. Various scenarios are explored based on fluctuations in solar irradiance and partial shading. Simulation results with real-time data confirm that the controllers perform satisfactorily under varying irradiance and partial shading conditions.

APPENDIX

Parameters of PV module

Simulation [40]	
Maximum power (P_{pvmax})	215.0W
Voc	36.9V
I_{sc}	8.01A
Voltage at P_{pvmax} (V_{mpp})	30.3V
Current at P_{pvmax} (I_{mpp})	7.10A
Number of modules connected in series (N)	22
Real time data [41]	
Module Type	TP280
P_{pvmax}	280.0W
Voc	44.0V
I_{sc}	8.28A
V_{mpp}	36.2V
I_{mpp}	7.73A
Efficiency	14.10%
Power tolerance	[-0 & +4.5]
N	4

Parameters of IM

Simulation [42]	
Power	5hp
Voltage	415 V
Stator current	7.9 A
Number of poles	4
Stator resistance	1.9 ohm
Stator inductance	0.1542 H
Real time data [43]	
Type of motor	KI100L
Power	3hp
Rated voltage	415 V
Rated current	4.7 A
Number of poles	4
Rated speed	1430 rpm

Parameters of P&O and MIWO

Step change in voltage (ΔV)	0.5
Maximum number of seeds (W_{max})	7

REFERENCES

[1] S. G. Malla et al., "Whale Optimization Algorithm for PV Based Water Pumping System Driven by BLDC Motor Using Sliding Mode Controller," in IEEE Journal of Emerging and Selected Topics in Power Electronics, vol. 10, no. 4, pp. 4832-4844, Aug. 2022, doi: 10.1109/JESTPE.2022.3150008.

[2] C. N. Bhende, S. G. Malla, "Novel Control of Photovoltaic based Water Pumping System without Energy Storage", *International Journal of Emerging Electric Power Systems,* vol. 13, no. 4, 2012.

[3] S. Sashidhar, V. G. P. Reddy, B. G. Fernandes, "A Single-Stage Sensorless Control of a PV-Based Bore-Well Submersible BLDC Motor," *IEEE Journal of Emerging and Selected Topics in Power Electronics*, vol. 7, no. 2, pp. 1173-1180, 2019.
[4] S. Sashidhar, B. G. Fernandes, "A Novel Ferrite SMDS Spoke-Type BLDC Motor for PV Bore-Well Submersible Water Pumps," *IEEE Transactions on Industrial Electronics*, vol. 64, no. 1, pp. 104-114, 2017.
[5] R. Kumar, B. Singh, "Single Stage Solar PV Fed Brushless DC Motor Driven Water Pump," *IEEE Journal of Emerging and Selected Topics in Power Electronics*, vol. 5, no. 3, pp. 1377-1385, 2017.
[6] K. K. Prabhakaran, A. Karthikeyan, S. Varsha, B. V. Perumal, S. Mishra, "Standalone Single Stage PV-Fed Reduced Switch Inverter Based PMSM for Water Pumping Application," *IEEE Transactions on Industry Applications*, vol. 56, no. 6, pp. 6526-6535, 2020.
[7] M. N. Ibrahim, H. Rezk, M. Al-Dhaifallah, P. Sergeant, "Solar Array Fed Synchronous Reluctance Motor Driven Water Pump: An Improved Performance Under Partial Shading Conditions," *IEEE Access*, vol. 7, pp. 77100-77115, 2019.
[8] S. Shukla, B. Singh, "Reduced-Sensor-Based PV Array-Fed Direct Torque Control Induction Motor Drive for Water Pumping," *IEEE Transactions on Power Electronics*, vol. 34, no. 6, pp. 5400-5415, 2019.
[9] M. J. M. Rao, M. K. Sahu, P. K. Subudhi, "PV based water pumping system for agricultural sector," *Materials Today: Proceedings*, vol. 5, no. 1, 1008-1016, 2018.
[10] J. V. Appen, M. Braun, Sizing and Improved Grid Integration of Residential PV Systems With Heat Pumps and Battery Storage Systems," *IEEE Transactions on Energy Conversion*, vol. 34, no. 1, pp. 562-571, 2019.
[11] A. Betka, A. Moussi, "Performance Optimization of a Photovoltaic Induction Motor Pumping System", *Renewable Energy*, vol. 29, no. 14, pp. 2167-2181, 2004, doi: 10.1016/j.renene.2004.03.016.
[12] M. Arrouf, N. Bouguechal, "Vector control of an Induction Motor fed by a Photovoltaic Generator", *Applied Energy*, vol. 74, no. 1-2, pp. 159-167, 2003, doi: 10.1016/S0306-2619(02)00142-3.
[13] J. R. Arribas, C. M. V. González, "Optimal Vector Control of Pumping and Ventilation Induction Motor Drives", *IEEE Transactions on Industrial Electronics*, vol. 49, no. 4, pp. 889-895, 2002, doi: 10.1109/TIE.2002.801240.
[14] A. Moghassemi, S. Padmanaban, V. Ramachandaramurthy, M. Mitolo, M. Benbouzid, "A Novel Solar PV fed TransZSI-DVR for Power Quality Improvement of Grid-Connected PV Systems," *IEEE Access*, vol. 9, pp. 7263-7279, 2021, doi:10.1109/ACCESS.2020.3048022.
[15] R. Toscano, P. Lyonnet, "A Kalman Optimization Approach for Solving Some Industrial Electronics Problems", *IEEE Transactions on Industrial Electronics*, vol. 59, no. 11, pp. 4456-4464, 2012, doi: 10.1109/TIE.2011.2169637.
[16] K. Ishaque, Z. Salam, M. Amjad, S. Mekhilef, "An Improved Particle Swarm Optimization (PSO)–Based MPPT for PV With Reduced Steady-State Oscillation", *IEEE Transactions on Power Electronics*, vol. 27, no. 8, pp. 3627-3638, 2012, doi: 10.1109/TPEL.2012.2185713.
[17] S. Yuantao, Z. Qing, "Based on the Cauchy Distribution Reproduce Mode Improved IWO Algorithm Research and Application", *in the 2nd International Conference on Information Science and Engineering (ICISE),* Hangzhou, China, pp. 1057-1060, 2010, doi: 10.1109/ICISE.2010.5690842.
[18] S. Karimkashi, A. A. Kishk, "Invasive Weed Optimization and its Features in Electromagnetics", *IEEE Transaction on Antennas and Propagation*, vol. 58, no. 4, pp. 1269-1278, 2010, doi: 10.1109/TAP.2010.2041163.
[19] M. A. Elgendy, B. Zahawi, D. J. Atkinson, "Comparison of Directly Connected and Constant Voltage Controlled Photovoltaic Pumping Systems", *IEEE Transactions on Sustainable Energy*, vol. 1, no. 3, pp. 184-192, 2010, doi: 10.1109/TSTE.2010.2052936.
[20] S. J. Chiang, K. T. Chang, C. Y. Yen, "Residential Photovoltaic Energy Storage System", *IEEE Transactions on Industrial Electronics*, vol. 45, no. 3, pp. 385-394, 1998, doi: 10.1109/41.678996.
[21] Handbook of secondary storage batteries and charge regulators in photovoltaic systems. Final report, report, *prepared by Exide Management and Technology Company*, West College Avenue, Yardley, Pennsylvania, US. 1981.
[22] http://www.irrigationtutorials.com/pump.htm
[23] R. Faranda and S. Leva, "Energy Comparison of MPPT techniques for PV Systems", *Journal of Electromagnetic Analysis and Applications*, vol. 3, pp. 446-455, 2008.
[24] T. Esram, P. L. Chapman, "Comparison of Photovoltaic Array Maximum Power Point Tracking Techniques", *IEEE Transactions on Energy Conversion*, vol. 22, no. 2, pp. 439-449, 2007, doi: 10.1109/TEC.2006.874230.
[25] A. R. Mehrabian, C. Lucas, "A Novel Numerical Optimization Algorithm Inspired from Weed Colonization", *Ecological Informatics*, vol. 1, no. 4, pp. 355-366, 2006, doi: 10.1016/j.ecoinf.2006.07.003.
[26] X, Yao, Y, Liu, G. Lin, "Evolutionary Programming Made Faster", *IEEE Transactions on Evolutionary Computation*, vol. 3, no. 2, pp. 82-102, 1999, doi: 10.1109/4235.771163.
[27] C. N. Bhende, S. Mishra, S. K. Jain, "TS-fuzzy-controlled active power filter for load compensation", *IEEE Transactions on Power Delivery,* vol. 21, no. 3, pp. 1459-1465, 2006, doi: 10.1109/TPWRD.2005.860263.
[28] B. K. Bose, "*Modern Power Electronics and AC Drives"*, PHI Learning, 2010.

[29] C. C. Chan, W. S. Leung, C. W. Ng, "Adaptive Decoupling Control of Induction Motor Drives", *IEEE Transactions on Industrial Electronics*, Vol. 37, No. 1, pp. 41-47, 1990, doi: 10.1109/41.45842.
[30] A. M. Bazzi, P. T. Krein, "Review of Methods for Real-Time Loss Minimization in Induction Machines", *IEEE Transactions on Industry Applications*, vol. 46, no. 6, pp. 2319-2328, 2010, doi: 10.1109/TIA.2010.2070475.
[31] A. M. Khambadkone, J. Holtz, "Vector-Controlled Induction Motor Drive with a Self-Commissioning Scheme", *IEEE Transactions on Industrial Electronics*, vol. 38, no. 5, pp. 322-327, 1991, doi: 10.1109/41.97551.
[32] G. O. Garcia, J. C. Mendes Luis, R. M. Stephan, E. H. Watanabe, "An Efficient Controller for an Adjustable Speed Induction Motor Drive", *IEEE Transactions on Industrial Electronics*, vol. 41, no. 5, pp. 533-539,1994, doi: 10.1109/41.315272.
[33] A. K. Abdelsalam, M. I. Masoud, M. S. Hamad, B. W. Williams, "Modified Indirect Vector Control Technique for Current-Source Induction Motor Drive", *IEEE Transactions on Industry Applications*, vol. 48, no. 6, pp. 2433-2442, 2012, doi: 10.1109/TIA.2012.2227132.
[34] J, Guzinski, H. Abu-Rub, "Speed Sensorless Induction Motor Drive with Predictive Current Controller", *IEEE Transactions on Industrial Electronics*, Vol. 60, No. 2, pp. 699-709, 2013, doi: 10.1109/TIE.2012.2205359.
[35] Z. Yan, C. Jin, V. I. Utkin, "Sensorless Sliding-Mode Control of Induction Motors", *IEEE Transactions on Industrial Electronics*, vol. 47, no. 6, pp. 1286-1297, 2000, doi: 10.1109/41.887957.
[36] M. Bhardwaj,"Sensorless Field Oriented Control of 3-Phase Induction Motors Using F2833x", *Application Report*, Texas Instruments Incorporated, 2013.
[37] http://www.fao.org/docrep/w7314e/w7314e0r.htm
[38] K. S. Jairaj, K. Srikant, "Simulation and Testing of Induction Motors Used with Irrigation Pumps", *International Journal of Automation and Power Engineering*, vol. 1, no. 2, pp. 23-28, 2012.
[39] A. M. Noman, K. E. Addoweesh, H. M. Mashaly, "DSPACE Real-Time Implementation of MPPT-Based FLC Method", *International Journal of Photoenergy*, vol. 2013, 549273, 2013, doi: https://doi.org/10.1155/2013/549273.
[40] http://www.trunsunsolar.com
[41] http://www.4-dgroup.com/4d/PDF/Tata%20300.pdf
[42] D. Ismail, A. Karem, M. Irwanto, N. Gomesh, M. Muzhar, M. Asri, "Parameters calculation of 5 HP AC induction motor" in *International Conference on Applications and Design in Mechanical Engineering (ICADME),* Batu Ferringhi, Penang, Malaysia, 2009.
[43] http://www.kirloskarpumps.com/download/prod_catalogue/Motor%20Catalogue.pdf